Electronic desalting for controlling the ionic environment in droplet-based biosensing platforms

Vikhram Vilasur Swaminathan, Piyush Dak, Bobby Reddy Jr., Eric Salm, Carlos Duarte-Guevara, Yu Zhong, Andrew Fischer, Yi-Shao Liu, Muhammad A. Alam, and Rashid Bashir

Articles you may be interested in

A high-throughput cellulase screening system based on droplet microfluidics
Biomicrofluidics **8**, 041102 (2014); 10.1063/1.4886771

Versatile on-demand droplet generation for controlled encapsulation
Biomicrofluidics **8**, 034112 (2014); 10.1063/1.4874715

A droplet-based novel approach for viable and low volume consumption surface plasmon resonance bio-sensing inside a polydimethylsiloxane microchip
Biomicrofluidics **7**, 044122 (2013); 10.1063/1.4819101

Cyclic olefin copolymer based microfluidic devices for biochip applications: Ultraviolet surface grafting using 2-methacryloyloxyethyl phosphorylcholine
Biomicrofluidics **6**, 012822 (2012); 10.1063/1.3682098

On-demand electrostatic droplet charging and sorting
Biomicrofluidics **5**, 024113 (2011); 10.1063/1.3604393

Electronic desalting for controlling the ionic environment in droplet-based biosensing platforms

Vikhram Vilasur Swaminathan,[1] Piyush Dak,[2] Bobby Reddy, Jr.,[3] Eric Salm,[4] Carlos Duarte-Guevara,[3] Yu Zhong,[3] Andrew Fischer,[5] Yi-Shao Liu,[6] Muhammad A. Alam,[2,a)] and Rashid Bashir[1,3,4,a)]

[1]*Department of Mechanical Science and Engineering, University of Illinois at Urbana-Champaign, Urbana, Illinois 61801, USA*
[2]*School of Electrical and Computer Engineering, Purdue University, West Lafayette, Indiana 47907, USA*
[3]*Department of Electrical and Computer Engineering, University of Illinois at Urbana-Champaign, Urbana, Illinois 61801, USA*
[4]*Department of Bioengineering, University of Illinois at Urbana-Champaign, Urbana, Illinois 61801, USA*
[5]*Abbott Laboratories, 1921 Hurd Drive, Dept. 8482 LC2 M/S 2-33, Irving, Texas 75038, USA*
[6]*Taiwan Semiconductor Manufacturing Company, Hsinchu 300-78, Taiwan*

The ability to control the ionic environment in saline waters and aqueous electrolytes is useful for desalination as well as electronic biosensing. We demonstrate a method of electronic desalting at micro-scale through on-chip micro electrodes. We show that, while desalting is limited in bulk solutions with unlimited availability of salts, significant desalting of ≥ 1 mM solutions can be achieved in sub-nanoliter volume droplets with diameters of $\sim 250\,\mu m$. Within these droplets, by using platinum-black microelectrodes and electrochemical surface treatments, we can enhance the electrode surface area to achieve $>99\%$ and 41% salt removal in 1 mM and 10 mM salt concentrations, respectively. Through self-consistent simulations and experimental measurements, we demonstrate that conventional double-layer theory over-predicts the desalting capacity and, hence, cannot be used to model systems that are mass limited or undergoing significant salt removal from the bulk. Our results will provide a better understanding of capacitive desalination, as well as a method for salt manipulation in high-throughput droplet-based microfluidic sensing platforms. © 2015 AIP Publishing LLC. [http://dx.doi.org/10.1063/1.4907351]

Background ions in electrolytes cause extensive shielding of charged molecules and surface potentials through the formation of the electrical double layer (EDL).[1–3] The Debye length,[4,5] λ_D, represents the phenomenological length-scale, which is the distance over which the potential from a charged surface decays to $\frac{1}{e}$ of its original value, and is given by

$$\lambda_D = \sqrt{\frac{\varepsilon k_B T}{2 N_A q^2 n_0}},\qquad(1)$$

where ε is the dielectric permittivity, k_B is the Boltzmann constant, T is the temperature, N_A is the Avogadro number, q is the fundamental electronic charge, and n_0 is the ionic strength of the electrolyte. Several common and physiological fluids, such as fresh water, brackish/saline waters, and blood/plasma, contain very high salt concentrations in the range of 5–500 mM. At the higher end of these concentrations, $\lambda_D < 1$ nm, and shielding effects are intense due to extreme crowding of counter-ions. When we look at applications involving the EDL, such as energy storage in supercapacitors,[6] capacitive deionization (CDI™),[7–9] or salt removal around nanowire FET biosensors to improve their sensitivity,[10,11] the actual capacity to absorb salt ions from a concentrated but finite background deviates far from predictions based on the idealization of dilute solution theory[5,12,13] for an EDL in equilibrium with an infinite bulk electrolyte.

In this letter, we address the problem of electronic desalting and identify certain geometric factors (viz., electrolyte volume, electrode area, and nano-structure topology) that constrain this effect within a droplet. Furthermore, we experimentally demonstrate enhancements to the EDL absorption using nano-textured electrodes for feasible desalting from high salt (≥ 10 mM) systems.

A schematic for localized electronic desalting is shown in Figure 1. On-chip metal microelectrodes are used to apply desalting voltage—$\Delta V_{Desalting}$ as shown in Figures 1(a) and 1(b). Figure 1(c) also shows micro-patterned electrodes (ca. $100\,\mu m \times 100\,\mu m$) and a microinjected droplet in air within which desalting can be performed. The electrodes are microfabricated by conventional evaporation and lift-off patterning of 1000 Å thick Ti/Pt films. The micro-droplet is stabilized in air by adding glycerol (13% by volume) to prevent evaporation of sub-nanoliter volumes.[14] In small quantities, glycerol does not adversely change the conductivity or the DC dielectric properties of the solution.[15] In an unbiased droplet, the spatial distribution of both positive, p, and negative ions, n, is uniform throughout, i.e., $n = p = n_0$ (Figure 1(a)), where n_0 is the initial background concentration. During desalting, some of these ions move from the bulk of the droplet to accumulate within the EDLs at the opposite polarity electrodes, respectively (Figure 1(b)). At sufficiently high applied bias and large electrode area, this causes substantial decrease in n and p from the rest of the droplet. The desalting bias is chosen below the electrolysis limit of 1.23 V to minimize side effects such as redox reactions, gas bubbling, and self-heating.[16]

a)Authors to whom correspondence should be addressed. Electronic addresses: rbashir@illinois.edu and alam@purdue.edu
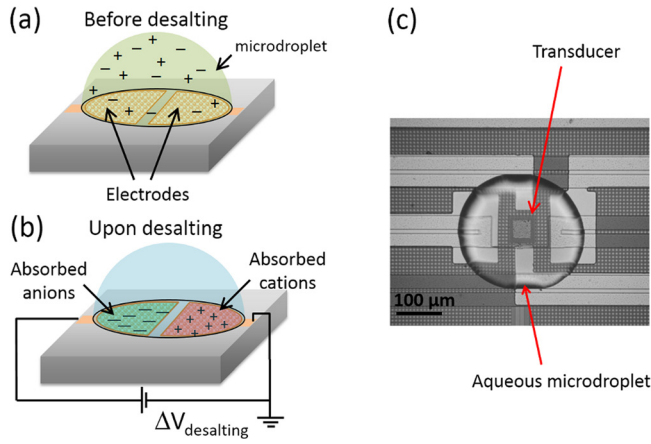
FIG. 1. Schematics (a) and (b) of electronic desalting in microdroplets. (b) By absorbing salt ions in the EDLs of desalting electrodes, the bulk of the droplet can be depleted. (c) Micrograph of two pairs of on-chip desalting electrodes patterned around a transducer and encapsulated within a droplet. The transducer's salt-dependent response can be modulated using this construct.

The surface charge density, σ_e, and potential, ψ, within the EDLs of very saline environments follow a highly non-linear relationship and the well-known exponential distribution from dilute solution theory breaks down.[17] Steric effects due to finite ion sizes at high ionic strength and large applied voltages are incorporated through Modified Poisson-Boltzmann (MPB) models,[18,19] in which ψ decays as follows:

$$\nabla \cdot (\varepsilon \nabla \psi) = -zq(p - n) = -zqn_i \frac{2 \sinh\left(\frac{zq\psi}{k_B T}\right)}{1 + 2\nu \sinh^2\left(\frac{zq\psi}{2k_B T}\right)}, \tag{2}$$

where z is the valency of ions, and n_i is the bulk ionic concentration away from the electrodes. The packing fraction, $\nu = 2n_i a^3$, accounts for finite size of the ions, a, so that ion density does not exceed $1/a^3$. For simplicity, we consider only the salt ions and neglect the contribution of H^+ and OH^- ions. Using the composite double layer approximation

of Kilic *et al.*,[17] we can derive an analytical expression for σ_e within the EDL of a system undergoing bulk desalting as follows:

$$\sigma_e = 4qn_0\lambda_0\sqrt{f}\sinh\left(\frac{qV_b}{2k_B T}\right) + \frac{ql_c}{a^3}, \tag{3}$$

where l_c denotes the thickness of the compact layer of maximum ion density, i.e., $1/a^3$ within the EDL, λ_0 is the initial Debye length, and $f = n_i/n_0$ is the desalting fraction. V_b is the potential drop across the Boltzmann layer, which depends on the electrode bias, V_e (refer to the supplementary material[20] for derivation). Note that in order to estimate σ_e from a microdroplet (300 pl) at an arbitrary bias, V_e, and initial concentration, n_0, Eq. (3) must be solved in a self-consistent manner. Further, to accurately determine the local ion concentration, we adopt a numerical model to solve for local values of ψ throughout the droplet and simulate the ion profiles for various salt concentrations. Details of the analytical derivation from MPB model, and the numerical scheme for solving ion profiles in droplets are discussed in the supplementary material.[20]

Ionic charge per unit area absorbed as a function of desalting bias is plotted for various ionic concentrations in Figure 2(a). The desalting efficiency of the system increases as expected with applied bias from 0 to 1.0 V. We also compare the self-consistent solution (solid lines) with the analytical predictions from the Gouy-Chapman (GC) point-charge model (dashed-dotted) and MPB solution (dashed). In low salt concentrations (10 µM), the exponential approximation of the GC model for σ_e is valid and agrees closely with the MPB model. The self-consistent solution differs from both semi-infinite model solutions because it is also constrained by limited availability of ions within the droplet. However, the MPB solution substantially deviates in high salt conditions ($\geq$1 mM), where the steric effects of ion crowding become dominant and the effect of large applied bias cannot be ignored. Double layer compaction occurs and is weakly dependent as $\sqrt{V_e}$ on the applied bias.[17] As a result, the EDL charge uptake capacity of electrodes decreases and lowers the desalting efficiency. The GC model over-predicts EDL
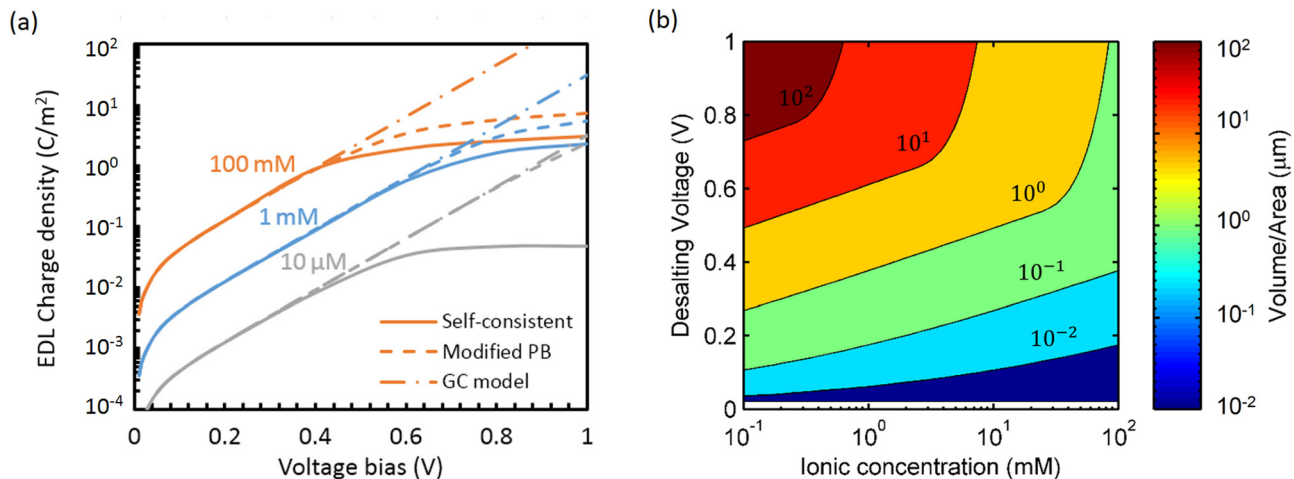

FIG. 2. Simulation of EDL charge density and desalting capacity. (a) EDL surface charge absorption capacity per unit area of desalting electrodes as predicted by various models. Conventional point charge theory begins to fail in high salt or large applied bias and self-consistent simulations further constrain the capacity. (b) Droplet volume-to-surface area ratios required for depleting 50% of the salt ions from various ionic strengths across a range of desalting bias. For appreciable desalting from $\geq$1 mM salt, nanostructured electrodes are necessary.
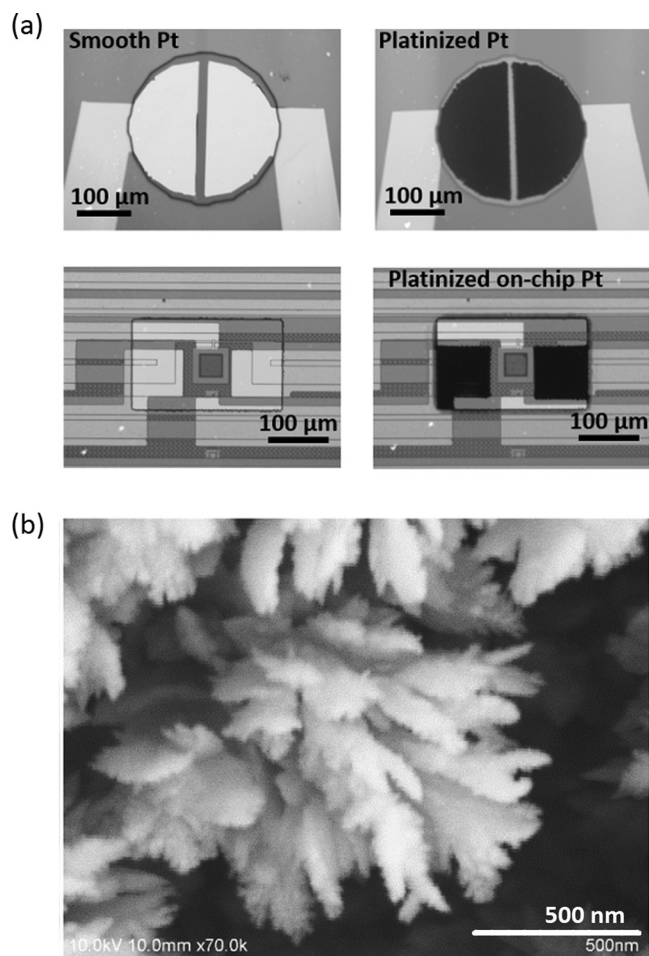
(a)

(b)

FIG. 3. Imaging of electrode surfaces. (a) Images of Platinum-black (HSA) microelectrodes patterned in test structures (circular electrodes as well as multi-electrode systems) through controlled electro-deposition process. (b) SEM image at high magnification (70 000×) shows a highly branched, dendritic nanostructure on the surface that leads to high surface area.

desalting capacity is significantly reduced. Under these circumstances, we can determine the maximum droplet volume, V_{max}, for a given electrode area, A_e, that can be desalted to a fraction f of the original salt concentration n_0,

$$\frac{V_{max}}{A_e} = \frac{8\sqrt{f}}{1-f}\lambda_0 \sinh^2\left(\frac{qV_b}{4k_BT}\right) + \frac{l_c}{n_0 a^3(1-f)}. \qquad (4)$$

Figure 2(b) shows the ratio of droplet volume to electrode area (V/SA) required for desalting droplets from various salt concentrations to a fraction $f = 0.5$. For desalting from small ionic concentrations (<1 mM), this ratio can be considerably large (V/SA $> 100\,\mu$m). However, for desalting from large ionic concentrations (~ 100 mM) below the reduction potential, we need V/SA $< 1\,\mu$m, which necessitates desalting in picoliter-sized droplets. Thus, in order to deplete more addressable droplet volumes (≥ 100 pl), we need electrodes of significantly higher surface area capable of increased ion absorption.

High surface area (HSA) platinum-black electrodes were prepared by electrodeposition methods,[21,22] using a Gamry Reference 600 Potentiostat (Gamry Instruments, PA, USA). Pt-black was galvanostatically deposited on a seed layer of 1000 Å thick Ti/Pt from dihydrogen hexachloroplatinate (0.08 mM $H_2PtCl_6\cdot6H_2O$, Sigma Aldrich, with 0.25 g/L of $(CH_3COO)_2Pb$, Alfa Aesar) at -0.08 A/cm^2 vs. Ag/AgCl. Decreasing the deposition current density helped with better process control for microelectrode tolerances ($\sim 10\,\mu$m). Figure 3(a) shows micrographs of Pt-black deposited on test electrodes in a circular well (250 μm diameter, 20 μm spacing between electrodes) and on-chip electrodes in a rectangular well (250 μm × 100 μm) around a transducer. SEM image of these electrodes (Figure 3(b)) confirms a highly branched, dendritic morphology, and the critical dimension in the nanostructure is of the order of ≤ 50 nm, which should provide the necessary area increase for desalting from high salt conditions.

We examined the surface area enhancement due to nanostructured HSA electrodes over smooth Pt by electrochemical impedance spectroscopy (EIS).[23–25] Figure 4(a)

charge absorption, and hence the desalting capacity, by nearly three orders of magnitude over the MPB solution. Furthermore, when we take into account the finite volume of the droplet, the self-consistent solution indicates that the
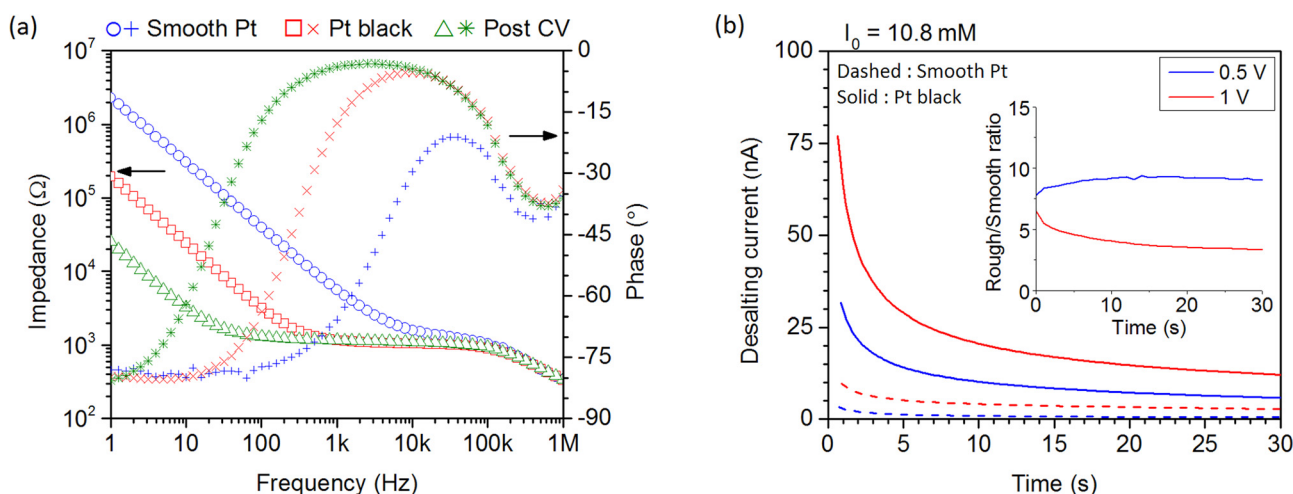

FIG. 4. Electrochemical characterization and performance testing of HSA electrodes. (a) EIS measurements show increased surface area available for desalting due to the nanostructures and subsequent improvement after cyclic voltammetry treatments that enable >100-fold available area increase. (b) Desalting current at 0.5 V and 1 V bias in nano-liter volume droplets show the increased ionic current flow due to the area enhancement of HSA electrodes over smooth electrodes. Inset shows the ratio of rough to smooth electrode transient at each time point.

TABLE I. Desalting capacities of various electrodes measured in bulk and micro-droplet.

Initial salt content	Percent salts depleted at 1 V desalting			Initial λ_D (nm)	Final λ_D (nm) HSA electrodes in droplet[b,c]
	Smooth electrodes in bulk (%)[a]	Smooth electrodes in droplet (%)[b]	HSA electrodes in droplet (%)[b,c]		
100 mM	0.0025	1.07	4.73	0.96	0.99
10.8 mM	0.16	6.85	41.41	2.93	3.82
1.17 mM	1.5	>99	>99	8.87	≫10

[a]Bulk volume was a large droplet of 0.1 μL.
[b]Micro-droplet diameter is 250 μm.
[c]HSA are high surface area Pt-black electrodes.

shows Bode plots of the impedance of circular test electrodes in bulk 1X PBS. Surface area increase from smooth Pt to Pt-black is reflected in the large decrease in impedance magnitude at 1 Hz, or *left-shifting* of the phase minima towards lower frequency because of the increase in EDL capacitance. By comparing the ratio of capacitances (imaginary component) or inverse ratio of resistances (real component), we observed that the *electrically available* increment was ca. 25-fold (see the supplementary material[20] for details of EIS analysis). The desalting capacity also increased for the test electrodes with the area enhancement, and we measured this within micro-droplets at various desalting voltages. Figure 4(b) shows ionic current traces in 10.8 mM 500 pl micro-droplets, at 0.5 V and I V desalting bias for both smooth and HSA electrodes. As depicted by the desalting current ratios (of HSA-over-smooth electrodes) in the inset of Figure 4(b), the desalting performance scaled by an order of magnitude from smooth Pt to Pt-black.

Although the physical area was dramatically enhanced (Figure 3(b)) and expected to provide two orders of magnitude improvement,[22] we only observed a limited increase during experiments. This may be attributed to either the incomplete coverage of the surface in contact with the droplet because of the increased surface energy cost of nanostructured surfaces that typically renders them repellant, or exclusion effects from steric issues that possibly come into play for ion absorption over a non-ideal surface as the roughness ($\leq$50 nm) approaches the phenomenological length-scale, λ_D. However, by conditioning the electrode surface through cyclic voltammetry (CV) treatment,[26] we can further improve and stabilize the surface characteristics of Pt-black for increased ion absorption during desalting. Test electrodes were cycled 5 times between -0.5 V and $+0.9$ V vs. Ag/AgCl at the rate of 100 mV/s in 1X PBS. From the EIS results (Figure 4(a)), we observed that the impedance at 1 Hz decreased further and the phase minima left-shifted to an even lower frequency. This translated to a 4-fold increase over the as deposited Pt-black so that, with CV treatment, the effective area of the electrodes increased by ca. 100-fold over smooth Pt.

Table I summarizes the desalting performance of both smooth and HSA electrodes through experimental measurements in bulk (large 0.1 μL volumes) as well as droplets (500 pL). In the bulk system, with smooth electrodes, we observed negligible salt removal from solutions that contained more than 1 mM of salt. This result agreed with our calculations (Figure 2) as V/SA ratio ($\gg$100) was extremely unfavorable

for desalting. The capacity improved as we approached the micro-droplet scale (V/SA $\sim$ 100), although it was only realistic for depleting at low concentrations ($<$10 mM). The HSA electrodes (V/SA $\sim$ 1), however, demonstrated significant salt removal and we were able to deplete $\sim$42% from 10 mM and $\sim$5% from 100 mM electrolytes. Note that this translates to ca. 30% increase in Debye length at 10 mM conditions, therefore electronic desalting can improve the response of transducers such as nanowire FETs (whose sensitivity varies logarithmically with salt concentration[10]) by perturbing at the biomolecular length-scales.

Our experimental results and self-consistent solution of desalting in droplets provide a better understanding of the practical limitations of EDL salt uptake in highly saline but limited-volume systems. The need for ultra-low profile volumes (V/SA $<$ 1) has ramifications for the energy density of EDL super-capacitors and the efficiency of CDI systems whose performance is typically overestimated by semi-infinite models. At the same time, we also provide a technique for electrode surface area enhancement, through nanostructured Pt-black and suitable surface conditioning, to achieve the desired value of V/SA $\sim$ 1 μm that enables feasible and substantial electronic desalting of more saline ($\geq$10 mM) micro-droplets. The droplet desalting construct can enable precise control of background salts around a FET biosensor and maximize its screening limited performance. Further improvements can be engineered to promote better wettability of nano-textured electrodes and spreading of even smaller droplet volumes in order to maximize the desalting capacity.

[1]M. Gouy, J. Phys. Theor. Appl. **9**, 457 (1910).
[2]D. L. Chapman, Philos. Mag. Ser. 6 **25**, 475 (1913).
[3]A. V. Delgado, F. González-Caballero, R. J. Hunter, L. K. Koopal, and J. Lyklema, Pure Appl. Chem. **77**, 1753 (2005).
[4]P. Debye and E. Hückel, Phys. Z. **24**, 185 (1923).

[5] A. J. Bard and L. R. Faulkner, *Electrochemical Methods: Fundamentals and Applications*, 2nd ed. (Wiley, New York, 2001).

[6] B. E. Conway, *Electrochemical Supercapacitors: Scientific Fundamentals and Technological Applications* (Plenum Press, New York, 1999).

[7] A. M. Johnson and J. Newman, J. Electrochem. Soc. **118**, 510 (1971).

[8] T. J. Welgemoed and C. F. Schutte, Desalination **183**, 327 (2005).

[9] M. Andelman, Sep. Purif. Technol. **80**, 262 (2011).

[10] P. R. Nair and M. A. Alam, Nano Lett. **8**, 1281 (2008).

[11] M. H. Sørensen, N. A. Mortensen, and M. Brandbyge, Appl. Phys. Lett. **91**, 102105 (2007).

[12] C. A. R. Perez, O. N. Demirer, R. L. Clifton, R. M. Naylor, and C. H. Hidrovo, J. Electrochem. Soc. **160**, E13 (2013).

[13] P. Simon and Y. Gogotsi, Nat. Mater. **7**, 845 (2008).

[14] E. Salm, C. D. Guevara, P. Dak, B. R. Dorvel, B. Reddy, M. A. Alam, and R. Bashir, Proc. Natl. Acad. Sci. U.S.A. **110**, 3310 (2013).

[15] R. Behrends, K. Fuchs, U. Kaatze, Y. Hayashi, and Y. Feldman, J. Chem. Phys. **124**, 144512 (2006).

[16] J.-H. Lee, W.-S. Bae, and J.-H. Choi, Desalination **258**, 159 (2010).

[17] M. Kilic, M. Bazant, and A. Ajdari, Phys. Rev. E **75**, 021502 (2007).

[18] A. Iglic and V. Kralj-Iglic, Electrotec. Rev. Slov. **61**, 127 (1994).

[19] I. Borukhov, D. Andelman, and H. Orland, Phys. Rev. Lett. **79**, 435 (1997).

[20] See supplementary material at http://dx.doi.org/10.1063/1.4907351 for analytical derivations from MPB model, numerical solutions of ion profiles in droplets, dye analysis of desalting profiles in microdroplets, and EIS analysis of various electrodes.

[21] R. S. Jayashree, J. S. Spendelow, J. Yeom, C. Rastogi, M. A. Shannon, and P. J. A. Kenis, Electrochim. Acta **50**, 4674 (2005).

[22] L. Zhu, N. Kroodsma, J. Yeom, J. L. Haan, M. A. Shannon, and D. D. Meng, Microfluid. Nanofluid. **11**, 569 (2011).

[23] *Impedance Spectroscopy: Theory, Experiment, and Applications*, 2nd ed., edited by E. Barsoukov and J. R. Macdonald (Wiley, Hoboken, New Jersey, 2005).

[24] J. Kang, J. Wen, S. H. Jayaram, A. Yu, and X. Wang, Electrochim. Acta **115**, 587 (2014).

[25] F. Heer, W. Franks, A. Blau, S. Taschini, C. Ziegler, A. Hierlemann, and H. Baltes, Biosens. Bioelectron. **20**, 358 (2004).

[26] L. Qiang, S. Vaddiraju, J. F. Rusling, and F. Papadimitrakopoulos, Biosens. Bioelectron. **26**, 682 (2010).